

RESEARCH ARTICLE

Numerical modelling and analysis of porous surface-enhanced jet cooling using copper inverse opals in single-phase flow

Shuhang Lyu¹, Qianying Wu² and Tiwei Wei^{1,*} 

¹School of Mechanical Engineering, Purdue University, West Lafayette, IN 47907

²Department of Mechanical Engineering, Stanford University, Stanford, CA 94305

*Corresponding author. E-mail: tiwei@purdue.edu

Received: 6 March 2023; **Revised:** 30 March 2024; **Accepted:** 31 March 2024

Keywords: Computational fluids dynamics; Impingement jet cooling; Porous media; Microelectronics; Surface enhancement

Abstract

In this study, we propose a novel cooling scheme that utilizes copper inverse opals (CIOs) for surface enhancement in a single-phase impingement jet cooling system. We perform computational fluid dynamics simulations to evaluate the cooling performance of the CIO jet coolers. Our modelling results indicate that the proposed CIO-coated cooler can significantly reduce the average temperature and improve the temperature uniformity across the entire chip surface. The average Nusselt number of the CIO-coated cooler can reach up to 2.8 times that of the flat surface jet cooler. However, the porous structure of the CIO-coated cooler increases the total pressure drop. To determine designs with high cooling performance and low energy consumption, we investigate two crucial design factors, namely the inlet velocity and the nozzle-to-CIO distance. Our analysis reveals that increasing the inlet velocity further enhances the heat transfer, but at the expense of high pressure drop. On the other hand, a larger nozzle-to-CIO distance results in a lower pressure drop but also reduces the heat transfer coefficient. The effects of nozzle-to-CIO distance are further understood by studying the flow resistance network. Furthermore, we present a reduced-order model that accurately captures the thermofluidic characteristics of the proposed design.

Impact Statement

With the increasing demand for high-performance microelectronics as well as high-power electronics applications, there is a need for advanced cooling technologies to mitigate the thermal challenges posed by high heat flux levels. Impingement jet cooling has emerged as a promising electronic cooling technique due to its high cooling efficiency and ability to achieve a uniform temperature distribution across the heating surface. In this study, copper inverse opals (CIOs) are integrated into the single-phase impingement jet cooling system for the thermal management of highly compact microelectronic devices. The results of this study have significant implications for the development of advanced cooling techniques that can enhance the performance and reliability of high-power microelectronics. Our study suggests values of design factors at which the cooler only brings about a slight pressure drop increase while maintaining a notable heat transfer enhancement. Our proposed model can serve as a valuable tool for designing CIO-based cooling systems.

1. Introduction

The miniaturization of electronic devices has led to an increase in heat flux, resulting in a notable impact on the electrical performance and reliability of such devices (Garimella 2006). As a result, thermal management has become a significant concern in microelectronics design. Conventional cooling methods, such as air coolers and fin heatsinks, are unable to meet the increasing demands for highly efficient heat removal methods in the semiconductor industry. The current trend of development shows a sustained growth of heat flux and a reduction of available space in closely packed systems (Abo-Zahhad *et al.* 2022). Therefore, innovative and advanced electronic cooling schemes that offer excellent heat removal capacity and cooling efficiency need to be explored. Among the available high-efficiency electronic cooling schemes, embedded microchannel and impingement jet cooling, have demonstrated great potential for dealing with the extremely high heat flux in highly compact microsystems.

Single-phase jet impingement has been established as a promising cooling scheme for highly integrated microdevices, based on both numerical and experimental investigations (Brunschwiler *et al.* 2006; Tang *et al.* 2016; Laguna *et al.* 2018; Patil & Hotta, 2018; Wei *et al.* 2019a,b, 2020a,b, 2022). Due to the thin hydrodynamic and thermal boundary layers generated by the impingement jet, single-phase liquid impingement jet cooling can achieve a much higher heat transfer coefficient (HTC) than conventional cooling schemes, particularly in the stagnation region. Sridhar (2013) compared the performances of different cooling solutions and found that the HTC of single-phase impingement jets is at least one order of magnitude larger than that of forced convection. Additionally, recent research by Wei *et al.* (2020a) demonstrated that single-phase water impingement jets can achieve an average HTC of up to $6 \times 10^4 \text{ W (K} \cdot \text{m}^2)^{-1}$ on the targeted surface. However, the non-uniformity of the HTC on the targeted surface remains a significant drawback of impingement single jet cooling (Bhunja, Chandrasekaran & Chen 2007), leading to a substantial temperature gradient along the chip surface and affecting device performance. To address this issue, a microjet array with distributed outlets has been proposed and demonstrated to be capable of significantly improving temperature uniformity while maintaining low pumping power (Wei *et al.* 2022). Nevertheless, although single-phase impingement jet cooling can achieve a high HTC, it might still be inadequate for state-of-art and future high-power devices with a localized heat flux of up to 1000 W cm^{-2} (Kandlikar & Bapat 2011).

Single-phase liquid impingement jet cooling is an active cooling method that can be further improved by using surface enhancements such as pillar-like (Chakroun, Abdel-Rahman & Al-Fahed 1998) or rib-like (Tan, Zhang & Xu 2014) fins, porous coatings (Wang *et al.* 2019) and local convexity (Kim, Afzal & Kim 2016). These surface structures can extend and increase the surface area for convective heat transfer but may also affect the system pressure drop and increase power consumption. Table 1 provides a summary of the surface enhancement methods for liquid impingement jet cooling reported in the literature. Of the different types of surface enhancements, porous coatings have shown remarkable improvement in heat transfer, and offer great potential for dealing with high heat flux in high-power devices (Wang *et al.* 2019). However, the high flow resistance in porous media can cause a large pressure drop, which may limit their practical use. Additionally, the size of the porous structure is limited to a larger pore size which can restrict the cooling efficiency. Therefore, it is crucial to carefully investigate the trade-offs between heat transfer enhancement and pressure drop when considering the use of porous coatings in liquid impingement jet cooling.

Copper inverse opals (CIOs) are microscale porous materials that have attracted extensive research interest due to their great potential in enhancing heat transfer, particularly in boiling heat transfer, by providing high-density nucleation sites (Lee *et al.* 2018). Copper inverse opals are porous structures deposited around a matrix of sacrificial microspheres with regular arrangements on a silicon substrate with a thin Au metal layer. The combination of copper's high thermal conductivity and the large surface-to-volume ratio of the inverse opal structure ensures excellent thermal conduction and convection in porous media, leading to superior heat transfer characteristics of CIOs. Furthermore, the interconnected pores in CIOs facilitate fluid transportation with high permeability, resulting in a lower pressure drop than the widely used sintered copper (Zhang *et al.* 2015). These superior heat transfer and flow characteristics

Table 1. Summary of surface enhancement methods for jet impingement cooling.

Reference	Coolant	Surface enhancement method	HTC improvement
Sullivan, Ramadhyani & Incropera (1993)	FC-77	Sawcut grid	150 %
Teuscher, Ramadhyani & Incropera (1993)	FC-77	Parallel plate fins/square array of pin fins	230 %–450 % (Plate) 200 % (Pin fin)
Copeland (1996)	FC-72	Pin fin array	300 %
Jeffers et al. (2009)	Water	Vane/Fins/Dish/Pedestal structures	120 % (Pedestal with turn-down)
Ndao et al. (2012)	R134	Micro pin fin array	203 %
Moreno et al. (2013)	Water	Microfinned/Microporous coating/Spray pyrolysis coating	100 % (Submerged jets)
Huang et al. (2017)	Water	Dimples	20 % (Convex dimples)
Wang et al. (2019)	Air	Copper foam	170 %
Tepe et al. (2020)	Air	Rib with extended jet holes	40.32 %

make CIOs promising materials for single-phase impingement jet cooling, particularly in high-power devices where high heat fluxes above 1000 W cm^{-2} need to be dissipated. However, the integration of CIOs with advanced cooling technologies requires further investigation to realize their full potential. Specifically, future research should focus on optimizing the design of CIOs, understanding the effects of impingement jet parameters and assessing the impact of CIOs on the overall system performance.

In this study, we investigate the potential of CIOs for use in single-phase impingement jet cooling systems through numerical simulations using computational fluid dynamics (CFD) simulations. A novel jet cooling design with alternating feeding and draining jets is highlighted in this study. The microscale jet cooling system with microporous structures is thoroughly studied, and is expected to have distinctive characteristics from systems at the macroscale due to the less confined jet spaces and the smaller pore size. The potency of CIOs in enhancing convection heat transfer and mitigating temperature non-uniformity on the chip interface is investigated.

In § 2, we present the methodology used in our numerical modelling, including details on the geometry, parameters, simulation method and parameter extraction. In § 3, we evaluate the cooling performance of a single-phase impingement jet cooler with CIOs and benchmark this by comparison with jet impingement on a flat chip surface. We assess the temperature profile on the chip interface and the average Nusselt number to demonstrate the benefits of CIOs on heat dissipation in the system. Additionally, we analyse the flow characteristics by visualizing the flow field and visualizing the system pressure drop. In §§ 3.1 and 3.2, we also examine the effects of different design factors, e.g. inlet velocity and nozzle-to-CIO distance. Furthermore, we propose a reduced-order model for the average Nusselt number and system pressure drop coefficient in § 3.3. The simulations and model presented in this work aim to enhance our understanding of the thermofluidic properties of CIOs in a single-phase cooling system and provide guidance for the design of active liquid cooling systems utilizing CIOs. The findings and models developed in this work can give insights into the thermofluidic characteristics in microscale jet cooling systems with porous media which have great potential for microelectronics cooling and the development of design guidelines for such cooling systems.

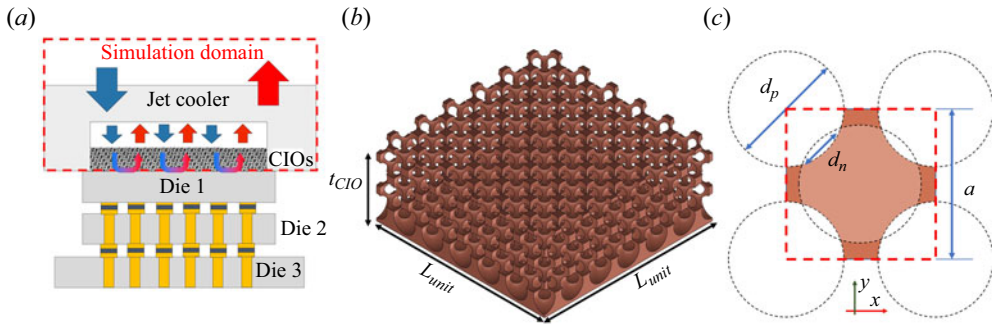


Figure 1. Impingement jet cooling with surface enhancement. (a) A layer of CIOs is fabricated on the backside of the chip. (b) The schematic of the CIO layer with dimensions of $L_{unit} \times L_{unit} \times t_{CIO}$. (c) Face-centred cubic unit cell structure with micropores in CIOs, critical parameter pore diameter d_p , neck diameter d_n and the lattice constant of the FCC structure a .

Table 2. Geometric parameters.

Parameter	Value
L_{unit}	70 μm
t_{CIO}	28 μm
d_p	9.0 μm
d_n	3.6 μm
a	11.7 μm
d_{in}	20 μm
I	0–15 μm

2. Methodology

2.1. Geometry and parameters

The schematic of the proposed cooling solution is depicted in [figure 1\(a\)](#), where the jet cooler with a nozzle array is placed on the backside of the stacked dies, providing multiple impingement jets. Instead of directly impinging on the die surface, a layer of CIOs is fabricated on the backside of the chip surface, where the jet arrays impinge on the porous layer and flow inside the CIO structure, facilitating enhanced convective heat transfer and efficiently removing the high heat flux from the chip. Deionized water is chosen as the working fluid in this study. The simulation domain is defined as shown in [figure 1\(a\)](#), where a constant heat flux boundary condition is applied on the bottom surface of the simulation domain. The nozzle plate geometry is illustrated in the top view of [figure 2\(a\)](#), where $N \times N$ inlets and $(N + 1) \times (N + 1)$ outlets are regularly arranged, forming a nozzle jet cooling array. To collect the returned liquid, a distributed return structure is designed and employed. To reduce computational time, a unit cell model is extracted from the nozzle array, which contains a one-fourth inlet and a one-fourth outlet, as illustrated in [figure 2\(b\)](#).

The design parameters of the proposed cooling solution are defined and summarized in [table 2](#). The unit cell model used in the numerical simulations consists of the length of the unit cell L_{unit} , inlet diameter d_{in} , outlet diameter d_{out} and nozzle-to-CIO distance I . The CFD model of the CIO structures with a thickness of t_{CIO} is shown in [figure 1\(b\)](#). The CIO layer is composed of spherical pores arranged in a face-centred cubic (FCC) structure, with interconnected necks between the pores, as shown in [figure 1\(c\)](#). The key structural parameters characterizing the CIOs include the pore diameter d_p , neck diameter d_n and lattice constant a of the FCC structure, as shown in [figure 1\(c\)](#).

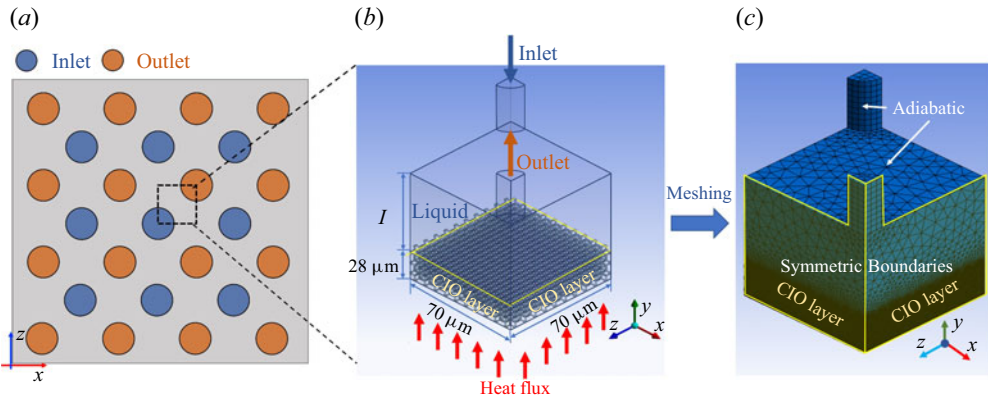


Figure 2. System set-up for the CFD simulations: (a) impingement jet cooling nozzle arrays with $N \times N$ inlet nozzles and $(N+1) \times (N+1)$ outlet nozzles. The jet array will be directly mounted on the top of the CIO surface. (b) Quarter CFD model and boundary conditions and (c) meshing of the unit cell. Symmetry boundary conditions are applied on the side surfaces of the unit cell. Heat flux (200 W cm^{-2}) is applied on the bottom surface to simulate the heat dissipated by the chip. Every single inlet is surrounded by four outlets.

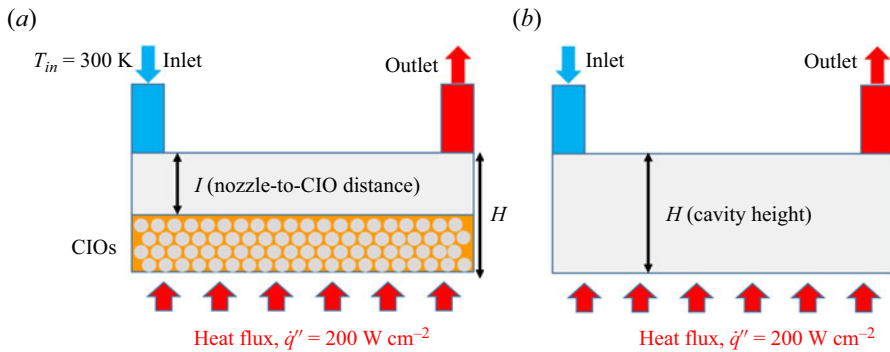


Figure 3. Schematics for jet impingement on (a) surfaces coated with CIOs and (b) flat surfaces without CIOs. The two cooling solutions are benchmarked and compared to illustrate the pros and cons of utilizing CIOs in single-phase impingement jet cooling.

2.2. Simulation method

In this study, we investigate the cooling performance of the proposed design through the evaluation of heat transfer and flow characteristics using CFD simulations on the Ansys 2022R2 platform. Figure 3 depicts the two different cooling schemes, namely impingement jet coolers with and without CIOs, to investigate the effects of the CIO coating on the thermofluidic characteristics and to benchmark the performance of the CIO-enhanced impingement jet cooling. For a fair comparison, all the conditions are kept the same for the two cooling schemes. The CFD simulations provide insights into the heat transfer enhancement and flow characteristics, offering valuable information to optimize the design and performance of the CIO-enhanced impingement jet cooling.

The flow regime of the inlet flow can be determined by evaluating the inlet Reynolds number

$$Re_{in} = \frac{u_{in} d_{in}}{\nu}, \quad (2.1)$$

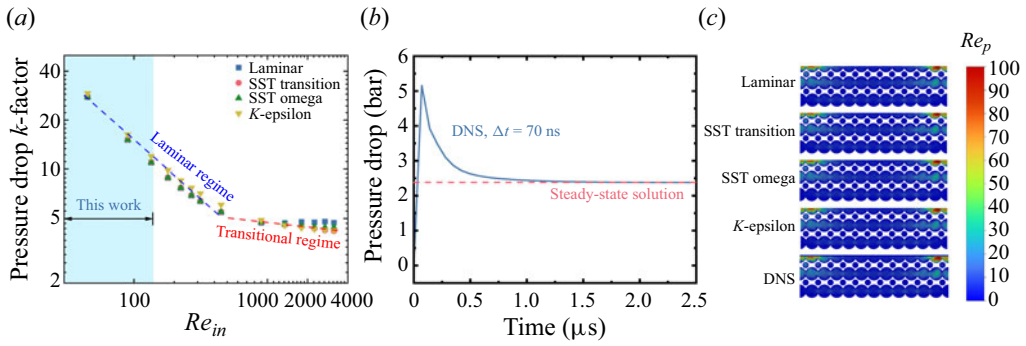


Figure 4. Transition of flow regimes using different turbulent models. (a) The dependence of pressure drop k -factor on the inlet Reynolds number is investigated with RANS models, showing a clear transition to the transition regime at $Re_{in} = 400$. The inlet Reynolds number in this work ranges from 20 to 160 and stays in the laminar regime. (b) The flow regime at $Re_{in} = 160$ is examined with transient DNS, showing a time-independent characteristic, and validating the laminar flow assumption. (c) Distribution of pore Reynolds number on the diagonal cross-section of the CIO layer. The velocity profile is associated with an inlet velocity of $u_{in} = 8 \text{ m s}^{-1}$, which is higher than all the cases in this paper. The distribution shows a maximum pore Reynolds number of $Re_p = 100$, which is significantly lower than the values for the transitional regime ($375 < Re_p < 750$).

where ν is the kinematic viscosity of the coolant, and u_{in} is the inlet velocity. Considering that the Reynolds numbers are far lower than the turbulent transition reported in the literature, which is often larger than 1000 (Zuckerman & Lior 2006), the impingement jet is treated as a laminar flow here. To justify the laminar assumption, the critical Reynolds number for the transition from the laminar to the transitional regime is identified with different Reynolds-averaged Navier–Stokes (RANS) models (Wei et al. 2019a). As shown in figure 4(a), the pressure drop k -factor is plotted at different inlet Reynolds numbers. The critical Reynolds number is assumed to be associated with the change of slope and is found to have a value of $Re_{in,cr} = 400$. The laminar assumption is verified by comparing the range of the inlet Reynolds number ($20 < Re_{in} < 160$) with the critical value ($Re_{in,cr} = 400$). In addition, a direct numerical simulation (DNS) is performed for the largest inlet Reynolds number, $Re_{in} = 160$, to confirm the flow regime with a transient simulation. The timestep is chosen as $\Delta t = 70$ ns, corresponding to a Courant–Friedrichs–Lewy (CFL) number of 1. As shown in figure 4(b), the flow becomes steady state after $2 \mu s$, indicating a time-independent laminar flow and showing a pressure drop value within 0.1% of the steady-state laminar solution. Additionally, in the DNS, the pressure drop approaches a constant value after $2 \mu s$. The time-independent pressure drop confirms the existence of the steady state, validating the steady-state assumption in our study. Moreover, although the laminar model is assumed to be able to capture the flow characteristics in porous media with small characteristic lengths (Ranut, Nobile & Mancini 2014), it is crucial to examine the local fluid characteristics inside the CIO structure to determine whether it is applicable here. The local Reynolds number inside the CIO layer is evaluated to check the flow regime inside the CIOs. A commonly used pore Reynolds number is defined based on the pore diameter

$$Re_p = \frac{\rho U d_p}{\mu}, \tag{2.2}$$

where ρ is the liquid density, and μ is the dynamic viscosity. The distribution of pore Reynolds number on the diagonal cross-section of the CIO structure under the largest flow rate condition, which corresponds to $u_{in} = 8 \text{ m s}^{-1}$ and a nozzle-to-CIO distance of $I = 1 \mu m$, is shown in figure 4(c). The contour of Re_p in figure S1(b) in the supplementary material available at <https://doi.org/10.1017/flo.1017/flo.2024.6> indicates that the pore Reynolds number ranges from 0 to 100 in this work. The pore

Reynolds number is significantly lower than the values for the transitional regime, which are reported to be $375 < Re_p < 750$ in the literature (Wood, He & Apte 2020).

The governing equations of the CFD simulations in this work are the Navier–Stokes equations with an assumption of steady state, incompressible fluid and neglecting viscous heating and gravity effects. The mathematical expression of the governing equations and the boundary conditions are as follows:

$$\text{Continuity equation:} \quad \nabla \cdot \mathbf{u} = 0, \quad (2.3)$$

$$\text{Momentum equations:} \quad \rho(\mathbf{u} \cdot \nabla)\mathbf{u} = -\nabla p + \mu \nabla^2 \mathbf{u}, \quad (2.4)$$

$$\text{Energy equation:} \quad \rho c_p (\mathbf{u} \cdot \nabla)T = k_f \nabla^2 T, \quad (2.5)$$

$$\text{Solid–liquid interfaces: (No-slip boundaries)} \quad \mathbf{u} = 0, \quad k_f \frac{\partial T}{\partial \mathbf{n}} = k_s \frac{\partial T}{\partial \mathbf{n}}, \quad (2.6)$$

$$\text{Side surfaces: (Symmetric boundaries)} \quad \mathbf{u} \cdot \mathbf{n} = 0, \quad \frac{\partial T}{\partial \mathbf{n}} = 0, \quad (2.7)$$

$$\text{Bottom surface: (Heat flux boundary)} \quad k_s \frac{\partial T}{\partial \mathbf{n}} = \dot{q}'', \quad (2.8)$$

$$\text{Other boundaries: (Adiabatic boundary)} \quad \mathbf{u} = 0, \quad \frac{\partial T}{\partial \mathbf{n}} = 0, \quad (2.9)$$

where \mathbf{u} is the velocity vector, \mathbf{n} is the normal vector of the surface, c_p is the heat capacity, \dot{q}'' is the heat flux on the bottom surface and k_f and k_s are the thermal conductivities of the fluid and solid, respectively.

The Ansys Fluent solver with quadratic upstream interpolation for convective kinematics differencing and the semi-implicit method for pressure linked equations algorithm is used to perform conjugate heat transfer and single-phase fluid dynamics simulations.

The flow characteristics in the porous structure are captured by fine meshing. As shown in figure 2(c), tetrahedral mesh cells with a maximum size of $0.5 \mu\text{m}$ are generated in the simulation domain. The mesh size is selected based on the mesh sensitivity analysis, as shown in figure S1 in the supplementary material. The system pressure drop and mean temperature of the chip interface (bottom surface of the CIO layer) are obtained at different mesh sizes, i.e. different numbers of elements. The result indicates that the effect of mesh size is negligible when the mesh size decreases to lower than $0.5 \mu\text{m}$. Therefore, a maximum mesh size of $0.5 \mu\text{m}$ is selected based on the computational time and simulation accuracy.

As shown in figure 2(b,c), different boundary conditions are applied according to the physical properties of the different interfaces. All side surfaces are specified as symmetric boundaries to characterize the nozzle array. All the interfaces between the solid and liquid domains are set as no-slip boundaries, which ensures a zero relative velocity at all the liquid–solid interfaces. The inlet is set to a liquid water inlet with a uniform velocity of u_{in} and a constant temperature of $T_{in} = 300 \text{ K}$, and a pressure outlet with a gauge pressure of 0 Pa is applied. A heat flux of $\dot{q}'' = 200 \text{ W cm}^{-2}$ is applied on the bottom surface of the unit cell model. The interfaces between the fluid and the cooler body, including the nozzle plate, inlet and outlet tubes, are assumed to be adiabatic. Previous work has demonstrated that the heat transfer through the solid cooler, which is denoted as ‘Jet cooler’ in figure 1(a), is negligible as the convection between fluids and the porous medium dominates in this scheme (Wei *et al.* 2020a). The cooler is pre-filled with liquid water, which is kept below the boiling temperature. As there is no gas phase in the cooling system, the surface tension effects originating from the liquid–gas interfaces are neglected here.

Our simulation results are first validated by comparing the Nusselt numbers of jets on flat surfaces with an analytical model proposed by Wei *et al.* (2022). As shown in figure 5, the simulation results coincide well with the theoretical model, which justifies the validity of our CFD simulation results.

The effects of two critical design factors, inlet velocity (u_{in}) and nozzle-to-CIO distance (I), are considered in this study. The inlet velocity significantly affects the thermofluidic characteristics of the cooler by varying the total flow rate and the impingement intensity. Different from the conventional jet cooling solution with a flat chip interface, the chip in the proposed design faces the impingement jet with a porous layer, which may lead to different fluid behaviour with increased jet velocity. It can be

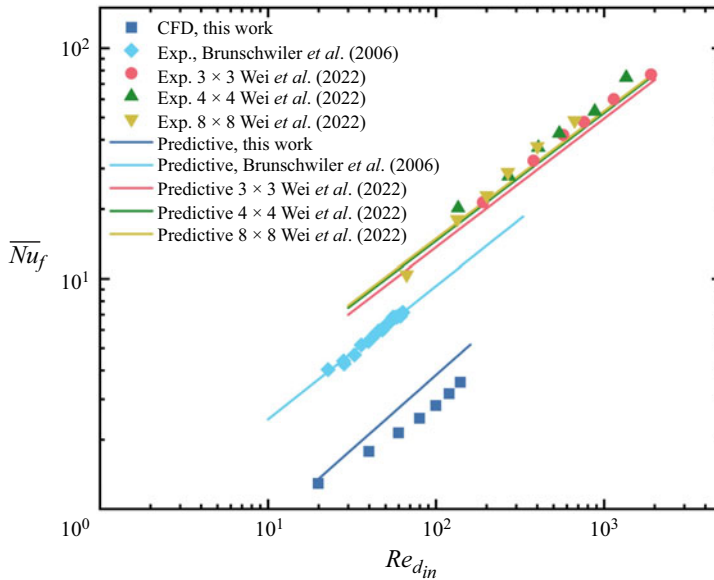


Figure 5. Comparison of theoretical model with experimental results and CFD simulations for jet on flat surfaces. All experimental data points are adopted from Wei et al. (2022) and Brunschwiler et al. (2006).

predicted that, as the inlet velocity increases, the impingement jet can reach a higher depth in the CIO layer, which may lead to better heat removal. Moreover, the system pressure drop is often closely related to the inlet velocity. Thus, the effects of inlet velocity on the pressure drop should be elucidated to achieve an energy-efficient design. Another critical design factor is the nozzle-to-CIO distance, which is defined as the distance between the inlet nozzle and the top surface of the CIO layer. The nozzle-to-CIO distance impacts the flow rate in the CIO layer and thus can have significant effects on the heat removal efficiency and pressure drop of the design. The details will be explained and discussed in § 3.

2.3. Parameters extraction

The performance of the cooling scheme is evaluated from two aspects, including the heat transfer and flow characteristics. The temperature profile on the chip interface is the crucial criterion for assessing the cooling solution as it remarkably impacts the reliability and performance of the cooled device. Therefore, the average Nusselt number, which represents the non-dimensional HTC of the impingement jet, is defined based on the average temperature of the chip interface and is used to characterize the heat transfer characteristics of the proposed design

$$\overline{Nu}_f = \frac{\dot{q}'' d_{in}}{(T_s - T_{in})k_f}, \tag{2.10}$$

where T_s is the area-averaged temperature of the chip interface, \dot{q}'' is the heat flux per unit area of the chip and k_f is the fluid thermal conductivity. Besides the average Nusselt number, the temperature uniformity of the chip interface is also studied by considering temperature variation on the chip interface, which will be further discussed below.

The flow characteristics of the system are critical in practice as they determine the required pumping power of the cooling solution, which can add to the total energy consumption of the electronic system and lower the energy efficiency. Hence, the pressure drop of the cooling scheme, i.e. the temperature difference between the inlet and the outlet, should be considered. The pressure drop is often normalized

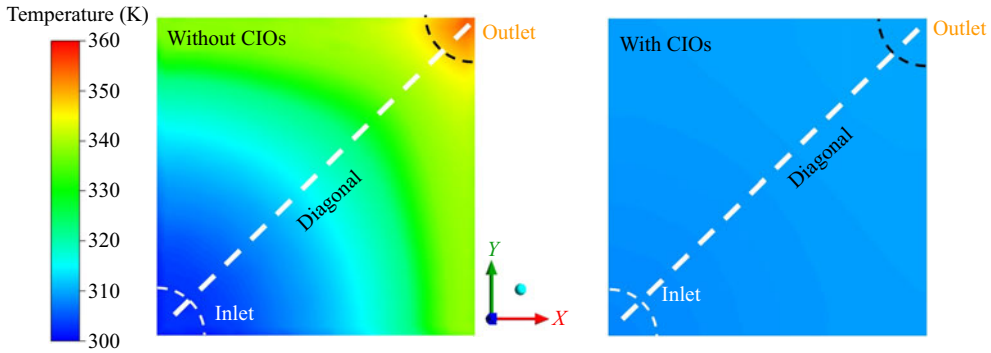


Figure 6. Temperature profile of the chip interfaces without and with CIO coatings. The CIOs significantly reduce the average temperature and the temperature non-uniformity of the chip interface. The temperature is obtained at $Re_{in} = 112$ and $l/L_{unit} = 0.07$.

as the pressure drop k -factor (Wei *et al.* 2022)

$$k = \frac{P_{in} - P_{out}}{\frac{1}{2}\rho u_{in}^2}, \quad (2.11)$$

where p_{in} and p_{out} are the pressure of the inlet and outlet fluid, respectively. Another critical concern for the CIO-enhanced jet cooler is the bypass flow phenomenon, which refers to the flow passing the cooler via the microchannel between the CIO layer and the nozzle due to the considerable flow resistance of the porous structure. As shown in figure S2(a) in the supplementary material, the inlet flow is divided into two parts, including the flow in the CIO layer and the microchannel between the CIOs and the cooler, which is called the bypass flow here. A large bypass flow rate can cause a low flow rate in the CIO layer and affect the effectiveness of the CIO coating. The ratio of the bypass flow rate to the total flow rate is defined as the bypass ratio, which indicates the strength of the bypass flow

$$\beta_b = \frac{4 \int_{A_{ref}} \mathbf{u} \cdot d\mathbf{A}_{ref}}{\pi d_{in}^2 u_{in}}, \quad (2.12)$$

where A_{ref} is the area of the reference plane, as shown in figure S2(b) in the supplementary material.

3. Results and discussion

3.1. Effects of jet velocity

The heat transfer characteristics of the cooler are first studied by analysing the temperature profile of the chip interface. As shown in figure 6, the temperature distribution is plotted at $Re_{in} = 112$ and $l/L_{unit} = 0.07$ to illustrate the typical temperature profiles with and without CIOs. The results indicate that the cooler with CIOs exhibits significantly lower temperatures and better temperature uniformity than the cooler without CIOs, which provides direct evidence of the superior performance of the jet cooler with CIOs. To further understand the heat transfer enhancement and the effects of the design factors, the heat transfer characteristics are analysed and compared at different inlet velocities ($Re_{in} = 20$ –140) and nozzle-to-CIO distances ($l/L_{unit} = 0.01$ –0.21).

The average Nusselt number is obtained for cooling schemes with CIOs and flat surfaces, allowing a more quantitative assessment of heat transfer characteristics. The results, shown in figure 7(a), indicate a substantial increase in the effective HTC of the cooler with the CIO layer, particularly at high inlet velocities. The Nusselt number of the cooler with CIOs is up to 2.8 times higher than that of the

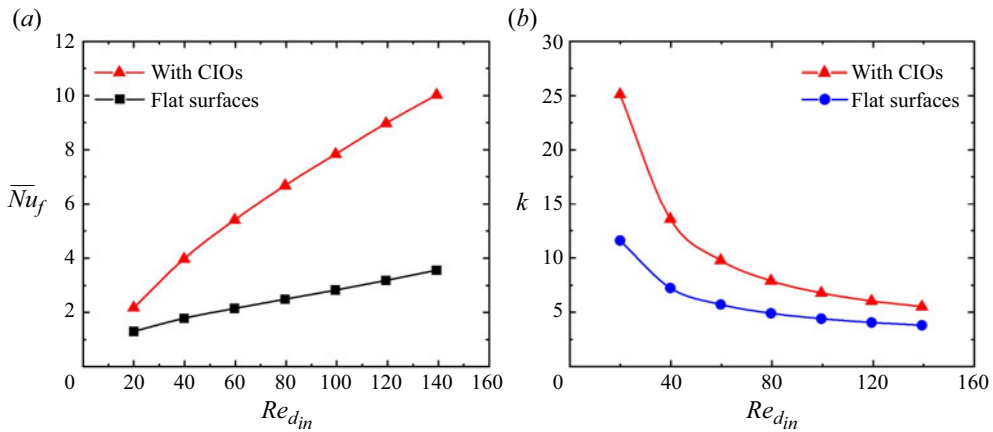


Figure 7. (a) Average Nusselt number based on the average temperature of the chip interface at different Reynolds numbers. (b) Pressure drop k -factor at different inlet Reynolds numbers.

cooler with a flat surface, demonstrating the significant enhancement in heat dissipation efficiency. The heat transfer enhancement can be attributed to the extended solid–fluid contacting surface area and the extraordinary heat conduction through solid copper in the CIO layer. Furthermore, it can be observed that the effects of CIOs on the heat transfer characteristics become more pronounced as the inlet velocity increases, supporting the hypothesis that higher impingement velocity drives the impingement jet deeper into the CIO structure.

Due to the horizontally connected structure of the CIOs, the heat transfer along the chip interface can be enhanced, contributing to temperature uniformity. The temperature distribution from the inlet to the outlet is plotted along the diagonal direction of the chip interface, which is indicated by the dotted line in figure 6, to assess temperature uniformity. As shown in figure 8, the temperature profile on flat surfaces is in line with previous works, indicating that heat is efficiently removed near the jet centre, leading to a low-temperature stagnation region. However, with the growth of the boundary layer, the HTC gradually decays along the flow direction, causing a temperature increase in the wall jet region. In contrast to the notable temperature gradient on the flat surfaces without CIOs, the temperature difference between the wall jet and the stagnation region is highly reduced on the CIO-coated surfaces, showing a much more uniform temperature distribution. In addition to promoting horizontal heat transfer, the uniform temperature profile may also be attributed to the thinner boundary layer developed in the porous structure, which can render a more uniform HTC distribution in the CIO layer and ensure a smaller temperature difference. Besides, it is also worth noting that, with the decrease in impingement velocities, the temperature difference between the maximum and minimum temperatures increases on flat surfaces while remaining almost the same on surfaces with CIOs. The diagonal temperature distributions are almost linear and constant on CIO-coated surfaces, which can maintain a uniform temperature even at low impingement velocities.

Although the CIO layer significantly enhances the cooling performance, an important concern for fluid systems with porous media is the increased pressure drop due to the high flow friction in the porous structure, which affects the energy consumption of the cooling solution and thus should be carefully considered. Therefore, the flow characteristics should be numerically studied to optimize the proposed design to achieve an appropriate pressure drop. Besides, as convective heat transfer is closely coupled with the fluid dynamics, the flow characteristics can improve the understanding of heat transfer characteristics.

The flow field is first visualized to show the flow characteristics in the systems with and without CIOs. Two specific conditions, i.e. a cooler with the liquid cavity filled with the CIO-coating and a cooler without CIOs, are compared here to show the impacts of the CIOs on the flow field. As shown

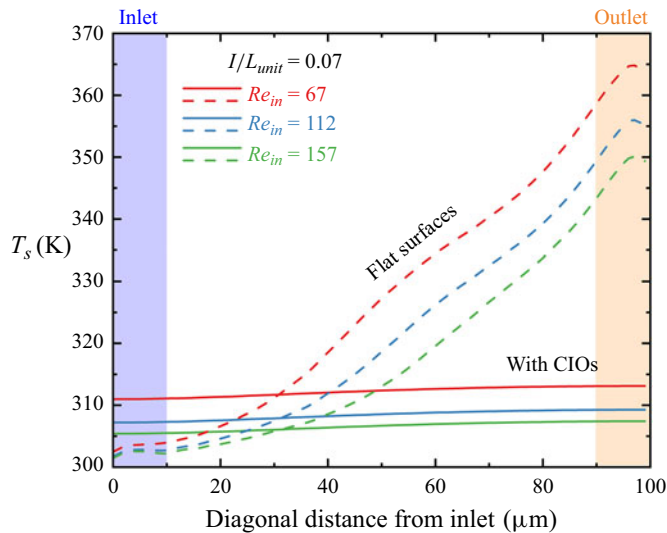


Figure 8. Diagonal temperature distribution of the chip interfaces at different inlet velocities. The smaller slopes on surfaces with CIOs indicate better temperature uniformity results from the horizontal heat conduction in the CIO structure.

in figure 9, the inlet fluid flows into the CIO layer and is rapidly redistributed in the porous structure. In contrast to the system with flat surfaces, no apparent stagnation region is observed on the CIO-coated surface as the flow friction in CIOs slows down the vertical jet and disperses the flow. The flow field shows that the CIO structure can redistribute the impingement jet among the CIO structure and thus enable a more uniform flow condition, which can give rise to the temperature uniformity of the chip, as mentioned above. However, the significant frictions of the porous structure may also induce a large pressure drop and thus lead to higher energy consumption.

The total pressure drops of the systems with and without CIOs are calculated and compared at different inlet velocities. As shown in figure 7(b), the pressure drop k -factor decreases with the inlet velocity in both systems. It is found that the existence of CIOs notably increases the system pressure drop at all the calculated inlet velocities. Moreover, it is noted that the difference between the pressure drop of the two systems becomes smaller at large jet velocities, which is assumed to be attributable to the dominant effects of flow frictions in the inlet and outlet nozzles at high flow rates.

3.2. Effects of nozzle-to-CIO distance

The nozzle-to-CIO distance (I) is another crucial design factor due to its significant effect on the heat transfer and flow characteristics of the cooler. Figure S2(a) (in the supplementary material) illustrates that the bypass flow space is affected by the nozzle-to-CIO distance. A larger distance can result in a stronger bypass flow, reducing the flow rate in the CIO layer and compromising the heat transfer enhancement effects of the CIOs. Conversely, decreasing the distance can improve heat dissipation. However, the variation in flow rate can affect the flow characteristics, which can influence the pressure drop. Here, both the average Nusselt number and the pressure drop are calculated and compared with jets on flat surfaces at different nozzle-to-CIO distances to quantitatively analyse the effects of the nozzle-to-CIO distance.

As shown in figure 10, as the nozzle-to-CIO distance decreases, the differences of both the pressure drop and the average Nusselt number are more significant between coolers with and without CIO coatings. The effects of the nozzle-to-CIO distance can be explained by analysing the flow resistance network from the inlet nozzle to the outlet nozzle. As shown in figure 11(a), a flow resistance network is

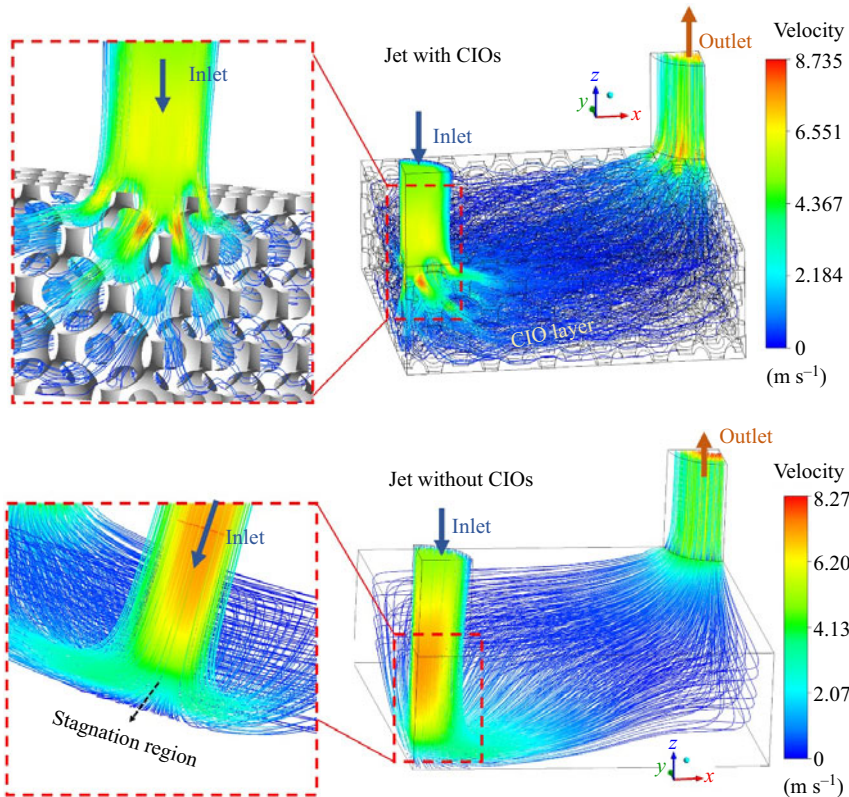


Figure 9. Visualization of the flow field for the jet on CIOs and on flat surfaces. An apparent stagnation region is observed in the jet cooler with flat surfaces. In contrast, when the jet impinges on the CIOs, the inlet fluid is redistributed in the porous structure, generating a more uniform flow.

sketched for the cooler, simplifying the flow resistance between the inlet nozzle and outlet nozzle as two parallel flow resistors, namely the flow resistance in the microchannel and the friction in the CIO layer. The flow resistances in the inlet and outlet tubes are considered invariant here as they mainly depend on the flow velocity and would not show notable variation at different nozzle-to-CIO distances. A lower nozzle-to-CIO distance can restrict the flow space in the microchannel and thus cause an increased flow resistance there. However, the flow resistance of the CIO layer remains the same as the CIO structure is invariant at different nozzle-to-CIO distances. According to the flow resistance network, an increase of flow resistance in the microchannel can drive more fluid to the CIO layer, enhancing the convective heat transfer and leading to a larger total pressure drop. In contrast, CIO-coated coolers with high nozzle-to-CIO distance only induce a slight pressure drop increase, but the low flow rate in the porous layer can weaken the heat transfer enhancement effects of CIOs. As mentioned before, we defined the bypass ratio to evaluate the strength of the bypass flow, i.e. the flow in the microchannel. Figure 11(b) shows that the calculated bypass ratios increase with the nozzle-to-CIO distance, which supports our assumption. As shown in figure 10, the CIO coating only shows minimal influence on the pressure drop when the nozzle-to-CIO distance exceeds $0.1 L$, suggesting that $H/L=0.1$ might be a good choice as it provides a relatively smaller pressure drop increase while maintaining a notable heat transfer enhancement.

3.3. Reduced-order model for CIO jet cooler

The above-mentioned factors, i.e. the inlet velocity and nozzle-to-CIO distance, play significant roles in practical design as they notably affect the heat transfer and flow characteristics and thus impact the

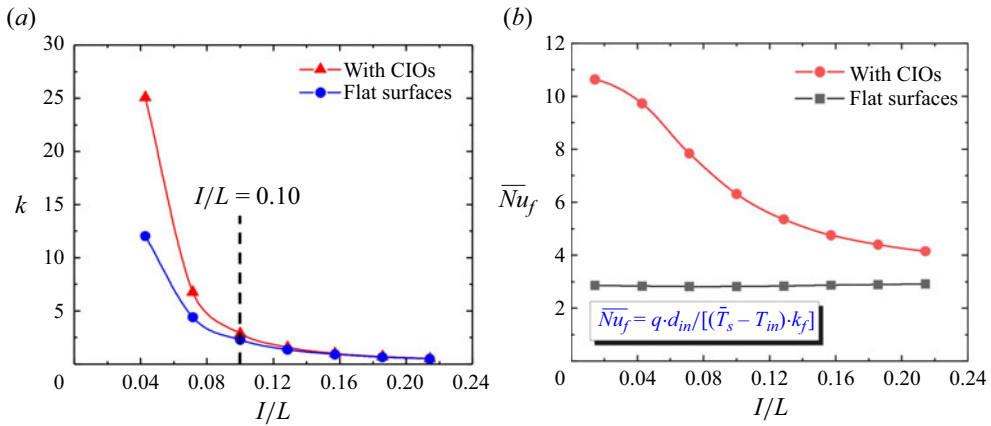


Figure 10. Effects of nozzle-to-CIO distance (I) on the thermofluidic characteristics. (a) The pressure drop k -factor at different nozzle-to-CIO distances. The variation in the pressure drop is negligible after the nozzle-to-CIO distance reaches $I/L = 0.1$. (b) The variation of average Nusselt number with nozzle-to-CIO distance. Heat transfer enhancement effect is weakened by the increased nozzle-to-CIO distance.

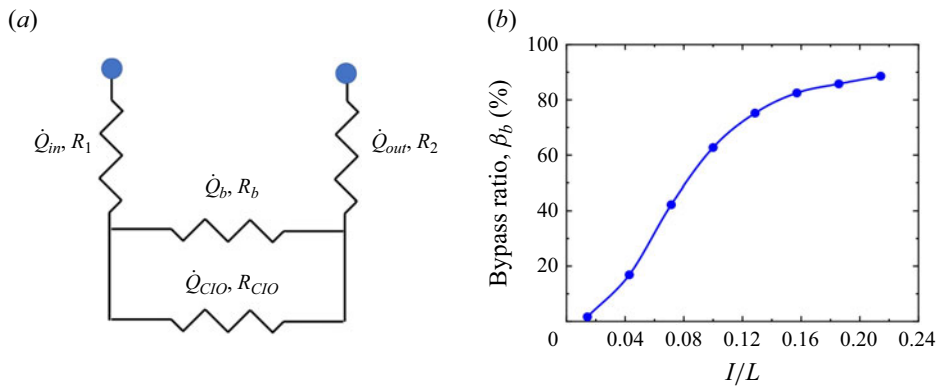


Figure 11. Influence of nozzle-to-CIO distance on the bypass flow rate. (a) Analysis of flow rate by using a flow resistance network. The flow is divided into two parts, the flow in the microchannel over CIOs and the flow in the CIO layer. (b) The bypass ratio increases with the nozzle-to-CIO distance, indicating a stronger bypass flow at a large nozzle-to-CIO distance.

performance of the cooler. An evaluation of the design metrics at different values of the design factors should be conducted to optimize the design to achieve highly efficient heat removal. However, CFD simulations are relatively time consuming, especially for systems with complex structures, and thus may be difficult to ensure a quick optimization of design parameters in wide ranges. Here, we propose a reduced-order model for two important design metrics of the CIO-coated jet cooler, namely, the average Nusselt number and the pressure drop, to capture the cooling performance. The model presents simple analytical correlations and thus allows easy optimization of the cooling design.

The fluid is assumed to flow in a diamond-shaped channel between the inlet and outlet. As shown in figure 12(a), the width of the channel is assumed to be wL_{diag} , where w is a fitting parameter and L_{diag} is the distance from the centre of the inlet nozzle to that of the outlet nozzle. The flow in the microchannel (the bypass flow) is assumed to be a laminar flow between parallel plates, and the flow in the CIO layer is considered as flow through a porous medium. The two flows are assumed to be parallel based on CFD simulation results. Hence, the vertical pressure drop can be neglected, indicating that the pressure

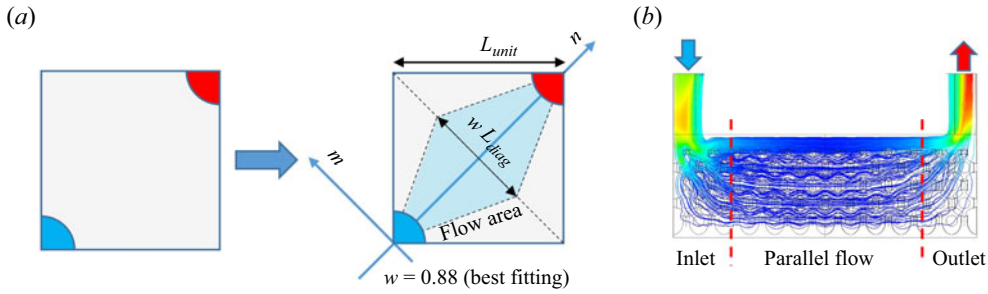


Figure 12. Modelling of the flow characteristics. (a) The flow area between the inlet and the outlet is assumed to be a diamond shape with a width of wL_{diag} . The parameter w is taken as $w = 0.88$ according to best fitting. (b) The pressure drop is divided into two parts, i.e. the pressure drop in the regions near the inlet and outlet nozzles and the parallel flow region away from the nozzles.

gradient along the flow direction can be expressed as

$$\left(\frac{dp}{dn}\right)_{CIO} = \left(\frac{dp}{dn}\right)_{bypass}, \tag{3.1}$$

where n is the coordinate along the flow direction. According to the conservation of mass for an incompressible fluid, the relationship between the average flow velocity for the bypass flow u_b and the superficial velocity of the CIO layer u_c can be written as

$$u_b A_b + u_c A_c = \dot{Q}_{in}, \tag{3.2}$$

where \dot{Q}_{in} is the inlet flow rate and A_b and A_c are the cross-sectional areas of the microchannel and the voids in the CIOs. A pressure gradient in a laminar flow between two parallel plates is called two-dimensional Poiseuille flow, which is a classical fluid mechanics problem and can be analytically solved as (Pelević & van der Meer 2016)

$$-\left(\frac{dp}{dn}\right)_{bypass} = \frac{3\mu}{(l/2)^2} u_b, \tag{3.3}$$

where μ is the dynamic viscosity of the fluid. Due to the absence of pressure drop correlations for inverse opals, a semi-empirical model for ceramic sponges is considered as the structure of the sponge is similar to CIOs. The pressure drop correlation by Dietrich (2013) is introduced here to describe the pressure gradient in the CIO layer

$$-\left(\frac{dp}{dn}\right)_{CIO} = 110 \frac{\mu}{\psi d_h^2} u_c + 1.45 \frac{\rho}{\psi^2 d_h} u_c^2, \tag{3.4}$$

where ψ is the porosity of the porous medium, ρ is the fluid density and d_h represents the hydraulic diameter, which is calculated as four times the cross-section available for flow divided by the wetted perimeter. Combining (3.1)–(3.4), the bypass ratio can be obtained as

$$\beta_b = \frac{u_b A_b}{u_b A_b + u_c A_c}. \tag{3.5}$$

The pressure drop of the system is divided into two parts, including the pressure drop in the region near the inlet and outlet nozzles and the pressure drop of the parallel flows, as shown in figure 12(b). The k -factor correlation proposed by Wei et al. (2022) is applied to calculate the pressure drop near the nozzles as it was stated that the majority of the pressure drop in a jet cooler comes from the region near

the nozzles. The pressure drop in the parallel flow region is calculated by integrating (3.4) along the flow direction. The system pressure drop can be expressed as

$$\Delta p = \frac{1}{2} k \rho u_{in}^2 - 2 \int_{R_{in}}^{L_{diag}/2} \left(\frac{dp}{dn} \right)_{CIO} dn. \quad (3.6)$$

The thermal conductivity of copper ensures a uniform temperature distribution along the horizontal direction, and thus the heat transfer is dominated by the vertical temperature gradient. The heat transfer characteristics are analysed by assuming a one-dimensional heat transfer in the vertical direction of the CIO layer. As shown in figure 13, the steady-state temperature of the CIOs is assumed to be merely dependent on the vertical coordinate z . A control volume with a thickness of dz is extracted from the CIO layer. According to energy balance, the control equation can be expressed as

$$k_{eff} \frac{\partial^2 T}{\partial z^2} - c_p (T_{out} - T_{in}) \dot{Q}_{in} \frac{dz}{V_{CIO}} = 0, \quad (3.7)$$

where c_p is the specific heat of fluid, T_{out} is the temperature of the fluid leaving the CIOs and k_{eff} is the effective thermal conductivity of the CIO layer

$$k_{eff} = \psi k_f + (1 - \psi) k_s, \quad (3.8)$$

where k_s and k_f are the thermal conductivities of the solid and fluid, respectively. Considering the convective heat transfer between the solid and liquid in the CIO layer, the leaving temperature of the fluid is related to the solid temperature by adopting the HTC in porous medium h_{CIO} proposed by Dietrich (2013)

$$h_{CIO} A_{CIO} \left(\frac{T_{in} + T_{out}}{2} - T \right) + k_{eff} V_{CIO} \frac{\partial^2 T}{\partial z^2} = 0, \quad (3.9)$$

where V_{CIO} is the total volume of the CIO layer, and A_{CIO} is the total area of fluid–solid interfaces in the CIOs. Combining (3.7) and (3.9), the temperature profile of the CIO layer can be solved as

$$r = \left. \begin{aligned} &T_s - T_{in} = A e^{-rz} + B e^{rz}, \\ &\frac{1}{k_{eff}} \frac{\rho \dot{Q}_{in} c_p \left(1 - \exp \left(-\frac{h_{CIO} A_{CIO}}{\rho \dot{Q}_{in} c_p} \right) \right)}{V_{CIO}} \end{aligned} \right\} \quad (3.10)$$

The constants A and B are obtained by considering the boundary conditions on the top and bottom surfaces of the CIO layer, which are set as a convection boundary and a constant heat flux boundary, respectively. For the convective heat transfer at the top surface of CIOs, the HTC on flat surfaces is calculated by the correlation proposed by Wei et al. (2022), which has been validated by comparison with experimental datasets, as shown in figure 5. The microchannel height above the CIO layer is taken as the cavity height for calculating the corresponding HTC.

The proposed analytical model has been compared with CFD simulation results to validate its effectiveness in predicting the heat transfer and flow characteristics of a CIO-coated jet cooler. As shown in figure 14, the reduced-order model is applied to calculate the pressure drop k -factor and average Nusselt number at different inlet velocities and nozzle-to-CIO distances. The results are consistent with the CFD simulation results. This validation demonstrates that the presented analytical model can be used to quickly and accurately optimize the design of the CIO-coated jet cooler. The reduced-order model can potentially save significant computational time and cost, making it a practical tool for engineers and researchers.

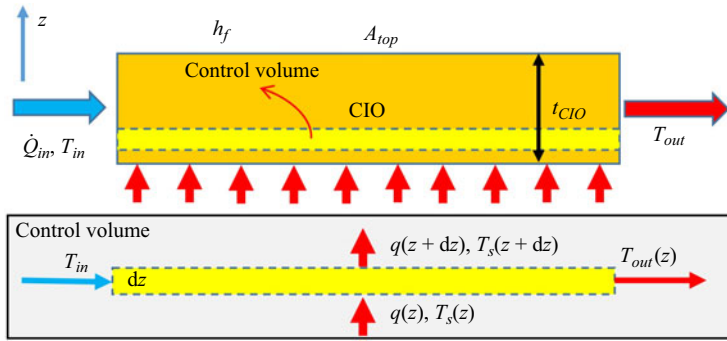


Figure 13. Heat transfer model for the CIO structure. The heat transfer is dominated by the vertical temperature gradient and thus is considered one-dimensional. A control volume with a thickness of dz is taken from the CIO layer to build up the control equation.

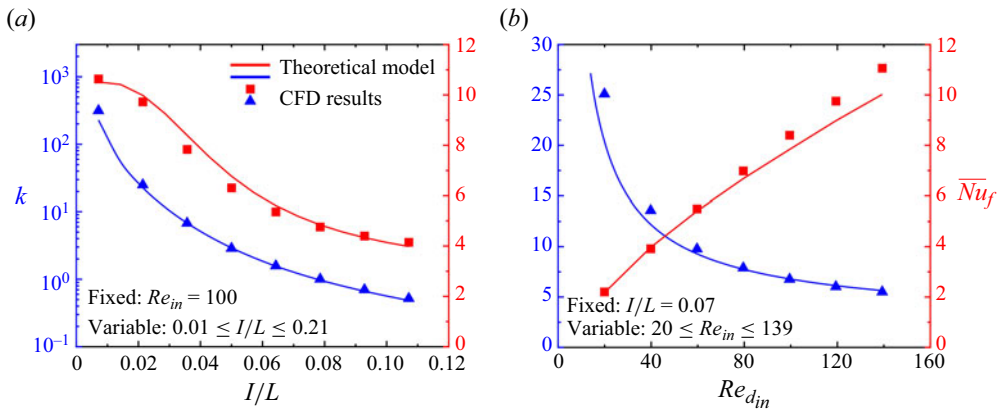


Figure 14. Validation of the reduced-order model. (a) The proposed model captures well the pressure drop k -factor and average Nusselt number at different nozzle-to-CIO distances. (b) The model also shows high accuracy in describing the thermofluidic characteristics at different inlet velocities.

4. Conclusions

In this study, we investigate the possibility of enhancing the cooling performance of single-phase impingement jet cooling solutions by integrating CIOs. Two design metrics, namely the average Nusselt number and the pressure drop k -factor of jet impingement cooling on CIO-coated surfaces, are benchmarked, and compared with those on flat surfaces to illustrate the pros and cons of CIO coating. The heat transfer and flow characteristics are further analysed to understand the underlying mechanisms of the CIOs effect. Additionally, we examine the impact of two crucial design factors, i.e. the inlet velocity and the nozzle-to-CIO distance, on the thermofluidic characteristics of the cooler. Furthermore, a reduced-order model is proposed to capture the thermofluidic characteristics of the cooler, allowing optimization of the design among a wide range of design parameters. Our study leads to the following key findings:

- (i) The synergy between CIOs and the distributed return structure greatly minimizes the non-uniformity of cooling and enhances the convective heat transfer, enabling a lower and more uniform temperature on the chip interface. However, the large flow resistance in CIOs will notably increase the total pressure drop of the jet cooler. Our study has shown that increasing the inlet velocity can effectively enhance the cooling performance of the jet cooler while mitigating the impact of the increased pressure drop caused by the CIOs.

- (ii) Increasing the nozzle-to-CIO distance results in a smaller flow resistance in the microchannel above the CIOs and thus leads to a stronger bypass flow and a lower flow rate in the CIO layer. The reduced flow rate in the porous layer decreases the pressure drop and the Nusselt number. A critical value of $I/L=0.1$ is observed, which only causes a slight pressure drop increase while maintaining a notable heat transfer enhancement.
- (iii) A reduced-order model is proposed to describe the pressure drop and average Nusselt number of jet coolers with CIOs. It provides analytical correlations for the design metrics and shows high accuracy in validation with the CFD simulation results. Application of the model can facilitate the optimization of cooler design and provide guidelines for the design of active cooling solutions with CIOs.

Overall, the use of CIOs in single-phase jet coolers offers a promising approach for improving chip cooling performance, but it is crucial to balance the cooling performance improvement against the associated increase in pressure drop. Further studies are required to explore the optimal operating conditions for CIO-coated jet coolers and to evaluate the long-term reliability of these systems.

Declaration of interests. The authors declare no conflict of interest.

Supplementary material. Supplementary material is available at <https://doi.org/10.1017/flo.2024.6>.

References

- ABO-ZAHHAD, E.M., AMINE HACHICHA, A., SAID, Z., GHENAI, C. & OOKAWARA, S. 2022 Thermal management system for high, dense, and compact power electronics. *Energy Convers. Manage.* **268**, 115975.
- BHUNIA, A., CHANDRASEKARAN, S. & CHEN, C.L. 2007 Performance improvement of a power conversion module by liquid micro-jet impingement cooling. *IEEE Trans. Compon. Packag. Technol.* **30** (2), 309–316.
- BRUNSCHWILER, T., ROTHUIZEN, H., FABBRI, M., KLOTER, U., MICHEL, B., BEZAMA, R.J. & NATARAJAN, G. 2006 Direct liquid jet-impingement cooling with micron-sized nozzle array and distributed return architecture. In *Thermal and Thermomechanical Proceedings 10th Intersociety Conference on Phenomena in Electronics Systems, 2006. IThERM 2006*, 196–203. IEEE. Available at: <https://doi.org/10.1109/ITHERM.2006.1645343>
- CHAKROUN, W.M., ABDEL-RAHMAN, A.A. & AL-FAHED, S.F. 1998 Heat transfer augmentation for air jet impinged on a rough surface. *Appl. Therm. Engng* **18** (12), 1225–1241.
- COPELAND, D. 1996 Single-phase and boiling cooling of small pin fin arrays by multiple nozzle jet impingement. *J. Electron. Packag.* **118** (1), 21–26.
- DIETRICH, B. 2013 Heat transfer coefficients for solid ceramic sponges – experimental results and correlation. *Intl J. Heat Mass Transfer* **61** (1), 627–637.
- GARIMELLA, S.V. 2006 Advances in mesoscale thermal management technologies for microelectronics. *Microelectron. J.* **37** (11), 1165–1185.
- HUANG, X., YANG, W., MING, T., SHEN, W. & YU, X. 2017 Heat transfer enhancement on a microchannel heat sink with impinging jets and dimples. *Intl J. Heat Mass Transfer* **112**, 113–124.
- JEFFERS, N.M.R., PUNCH, J., WALSH, E.J. & MCLEAN, M. 2009 Heat transfer from novel target surface structures to a normally impinging, submerged and confined water jet. *J. Therm. Sci. Engng Appl.* **1** (3), 1–9.
- KANDLIKAR, S.G. & BAPAT, A.V. 2011 Evaluation of jet impingement, spray and microchannel chip cooling options for high heat flux removal. *Heat Transfer Engng* **28** (11), 911–923.
- KIM, S.M., AFZAL, A. & KIM, K.Y. 2016 Optimization of a staggered jet-convex dimple array cooling system. *Intl J. Therm. Sci.* **99**, 161–169.
- LAGUNA, G., *et al.* 2018 Numerical parametric study of a hotspot-targeted microfluidic cooling array for microelectronics. *Appl. Therm. Engng* **144**, 71–80.
- LEE, H., MAITRA, T., PALKO, J., KONG, D., ZHANG, C., BARAKO, M. T., WON, Y., ASHEGHI, M., & GOODSON, K. E. (2018). Enhanced heat transfer using microporous copper inverse opals. *J. Electron. Packag. Trans. ASME*, **140**(2), 020906. <https://doi.org/10.1115/1.4040088/367979>
- MORENO, G., NARUMANCHI, S., VENSON, T. & BENNION, K. 2013 Microstructured surfaces for single-phase jet impingement heat transfer enhancement. *J. Therm. Sci. Engng Appl.* **5** (3), 031004. <https://doi.org/10.1115/1.4023308/379175>
- NDAO, S., LEE, H.J., PELES, Y. & JENSEN, M.K. 2012 Heat transfer enhancement from micro pin fins subjected to an impinging jet. *Intl J. Heat Mass Transfer* **55**, 413–421.
- PATIL, N.G. & HOTTA, T.K. 2018 A review on cooling of discrete heated modules using liquid jet impingement. *Front. Heat Mass Transfer* **11**, 1–13. <https://doi.org/10.5098/HMT.11.16>
- PELEVIĆ, N. & VAN DER MEER, T.H. 2016 Heat transfer and pressure drop in microchannels with random roughness. *Intl J. Therm. Sci.* **99**, 125–135.

- RANUT, P., NOBILE, E. & MANCINI, L. 2014 High resolution microtomography-based CFD simulation of flow and heat transfer in aluminum metal foams. *Appl. Therm. Engng* **69** (1–2), 230–240.
- SRIDHAR, A. 2013 Single phase and boiling heat transfer under steady and pulsating confined jet impingement. PhD dissertation, Department of Mechanical Engineering, Curtin University, Perth.
- SULLIVAN, P.F., RAMADHYANI, S. & INCROPERA, F.P. 1993 Use of smooth and roughened spreader plates to enhance impingement cooling of small heat sources with single circular liquid jets. *ASME-Publications-HTD* **206**, 103–110.
- TAN, L., ZHANG, J.Z. & XU, H.S. 2014 Jet impingement on a rib-roughened wall inside semi-confined channel. *Intl J. Therm. Sci.* **86**, 210–218.
- TANG, G., HAN, Y., LAU, B.L., ZHANG, X. & RHEE, D.M. 2016 An efficient single phase liquid cooling system for microelectronic devices with high power chip. *Proceedings of the Electronic Packaging Technology Conference, EPTC, 2016-February*. Available at: <https://doi.org/10.1109/EPTC.2015.7412300>
- TEPE, A.Ü., UYSAL, Ü., YETİŞKEN, Y. & ARSLAN, K. 2020 Jet impingement cooling on a rib-roughened surface using extended jet holes. *Appl. Therm. Engng* **178**, 115601.
- TEUSCHER, K.L., RAMADHYANI, S. & INCROPERA, F.P. 1993 Jet impingement cooling of an array of discrete heat sources with extended surfaces. *ASME-Publications-HTD* **263**, 1–10.
- WANG, J., KONG, H., XU, Y. & WU, J. 2019 Experimental investigation of heat transfer and flow characteristics in finned copper foam heat sinks subjected to jet impingement cooling. *Appl. Energy* **241**, 433–443.
- WEI, T., OPRINS, H., CHERMAN, V., BEYNE, E. & BAELMANS, M. 2019a Conjugate heat transfer and fluid flow modeling for liquid microjet impingement cooling with alternating feeding and draining channels. *Fluids* **4**, 145.
- WEI, T., OPRINS, H., CHERMAN, V., BEYNE, E. & BAELMANS, M. 2020a Experimental and numerical investigation of direct liquid jet impinging cooling using 3D printed manifolds on lidded and lidless packages for 2.5D integrated systems. *Appl. Therm. Engng* **164**, 114535.
- WEI, T., OPRINS, H., CHERMAN, V., BEYNE, E. & BAELMANS, M. 2020b Low-cost energy-efficient on-chip hotspot targeted microjet cooling for high-power electronics. *IEEE Trans. Compon. Packag. Manuf. Technol.* **10** (4), 577–589.
- WEI, T., OPRINS, H., CHERMAN, V., VAN DER PLAS, G., DE WOLF, I., BEYNE, E. & BAELMANS, M. 2019b Experimental characterization and model validation of liquid jet impingement cooling using a high spatial resolution and programmable thermal test chip. *Appl. Therm. Engng* **152**, 308–318.
- WEI, T., OPRINS, H., FANG, L., CHERMAN, V., BEYNE, E. & BAELMANS, M. 2022 Heat transfer and pressure drop correlations for direct on-chip microscale jet impingement cooling with alternating feeding and draining jets. *Intl J. Heat Mass Transfer* **182**, 121865.
- WOOD, B.D., HE, X. & APTE, S.V. 2020 Modeling turbulent flows in porous media. *Annu. Rev. Fluid Mech.* **52**, 171–203.
- ZHANG, C., RONG, G., PALKO, J.W., DUSSEAU, T.J., ASHEGHI, M., SANTIAGO, J.G. & GOODSON, K.E. 2015 Tailoring of permeability in copper inverse opal for electronic cooling applications. *ASME 2015 International Technical Conference and Exhibition on Packaging and Integration of Electronic and Photonic Microsystems, InterPACK 2015, Collocated with the ASME 2015 13th International Conference on Nanochannels, Microchannels, and Minichannels*, 2, V002T06A004. Available at: <https://doi.org/10.1115/IPACK2015-48262>
- ZUCKERMAN, N. & LIOR, N. 2006 Jet impingement heat transfer: physics, correlations, and numerical modeling. *Adv. Heat Transfer* **39**, 565–631.